The International Journal of Advanced Manufacturing Technology (2019) 102:3839–3848
https://doi.org/10.1007/s00170-019-03448-0

ORIGINAL ARTICLE

Hot-wire GTAW cladding: inconel 625 on 347 stainless steel

Bishal Silwal[1] · **James Walker**[1] · **Daniel West**[1]

Received: 17 December 2018 / Accepted: 12 February 2019 / Published online: 1 March 2019

Abstract
Gas tungsten arc (GTA) cladding has been widely applied in surface modification and repairing. In this study, low current gas tungsten arc welding (GTAW) cladding in the range of 60 to 100 A was performed with resistively heating hot-wire filler Inconel alloy (IN625) on the 347 stainless steel substrate. A 70 A or more primary current can be used to clad a continuous and uniform layer on the substrate by resistively heating the wire and varying the torch angle. Lower dilution and higher contact angle were observed for lower current clad. An analytical model has been used to understand the resistively heating hot-wire effect. The microstructure of the clad bead and the substrate was analyzed. A heat-affected zone (HAZ) cracking was observed in the higher range of primary current. An EDX analysis was performed to reveal iron (Fe) elemental dilution and elemental segregation.

Keywords 347 stainless · GTAW · Cladding · Inconel 625 · Additive manufacturing

1 Introduction

Cladding (coating or hardfacing) is an additional layer of a metallic alloy with certain thickness bonded to the substrate in order to improve the performance of the parts in service. The requirements of low dilution and low heat input have lead the cladding community to use high-power density sources such as laser and electron beam alternative to the arc welding power source. The use of such power sources will melt the wire or powder along with the substrate to generate the desired layer thickness and metallurgical bonding. Although the use of laser as a power source with wire is a promising and emerging technology, it offers less advantages compared to gas tungsten arc welding (GTAW) in terms of cost saving and productivity. The use of GTAW as a power source in the past has limited its use due to being high heat input process in surface cladding where less distortion and less dilution are desired. Xu et al. [1] have used the wire and GTAW power (120 A and 1 mm/s of travel speed) as well as the laser power; their results confirmed the higher dilution ratio with GTAW (41–46%) compared to laser power (4–7%). The cold-wire feeding in GTAW will utilize the radiating heat from the substrate as well as the arc to melt the molten metal, thus a low amperage range lesser than 120 A is not sufficient to clad with cold-wire GTAW. By pre-heating the wire, the wire can be melted with lower primary arc current, making hot-wire GTAW technologically viable for cladding application. For welding current of equal or higher than 120 A, feeding of a pre-heated wire will allow the deeper penetration as suggested by [2]; however, this may not hold true if the primary current is lowered with same travel and wire feed speed.

The lower primary current and thus the lower heat input have significance in engineering design application, for, e.g., cladding on a slotted channel as shown in Fig. 1, where the over melting of these slotted channels (recess) may not be adequate for the intended application. Another important requirement is the cladding on the 347 stainless steel to avoid liquation cracking in the partially melted zone (PMZ). A 347 stainless steel is a niobium-stabilized austenitic stainless steel which provides resistance to carbide precipitation and creep deformation. Because of such properties, the 347 stainless steel have been used in high-temperature applications like boilers, superheaters, and nuclear reactors [3]. From a processing point of view, an optimum heating rate in the heat-affected zone (HAZ) is required to avoid particle dissolution and thus constitutional liquation [4]. Also, the elemental dilution of ferrous alloy on the surface is important for corrosion and wear protection.

✉ Bishal Silwal
bsilwal@georgiasouthern.edu

[1] Mechanical Engineering Department, Georgia Southern University, 201 Forest Drive, Statesboro, GA 30458, USA

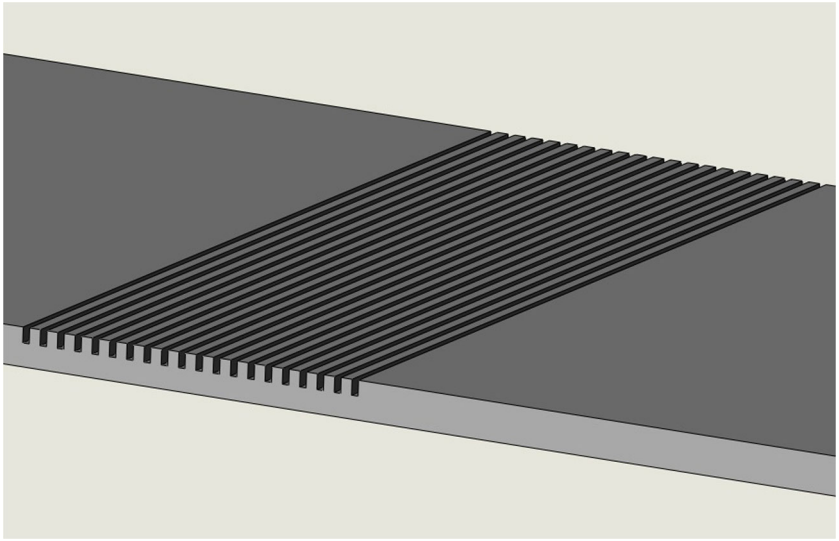

Fig. 1 The application of low current cladding on a groove channel. The slot is 1.0 mm wide and 2.5 mm high; each slot is 3 mm apart

Nickel-based superalloy (IN625) has been used extensively as a clad layer to protect against the corrosion in oil and gas industry [5] as well as high-temperature corrosive environments [6]. The IN625 also offers high creep and fatigue strength [7], thus it has been utilized heavily by surface modification industry. Based upon the available literature, laser and wire cladding [8] have shown that with 1.2-kW laser power and traverse speed of 3.3 mm/s, a 6.7-mm/s wire feed rate can be achieved without any significant problems into the bead appearance and dilution. With low energy input (less than 1.2 kW), the major issues were the wire stubbing and wire dripping [8]. Sandhu et al. [9] showed depositing Inconel 625 on 25-mm-thick 304 stainless steel using shielded metal arc welding (SMAW), using average welding speed of 2.34 mm/s and different ranges of welding current. An average dilution level of 35% was reported with the SMAW process. Pajukoski et al. [10] studied the corrosion performance using laser hot-wire and found better corrosion properties of IN625. Lv et al. [11] used resistively heating wire as well as primary current in the range of 210–270 A to achieve 50-mm/s wire feed speed; no travel speed was provided and the scope was limited to study the dissolution of Fe in copper. Recently, Gunther et al. [12] used hot-wire assisted gas metal arc welding (GMAW) and achieved a lower dilution rate of 10% using hypereutectic FeCrC hardfacing alloys. Thus, this research arises from the limited research available on these area: mainly cladding IN625 on 347 stainless steel. Ideally, it is worth investigating the process parameter window using restively heating hot-wire and the minimum heat input to successfully clad a continuous and uniform layer. In this respect, it is critical to understand and limit the hot-wire effect as well as lower the heat input and improve productivity. This paper reports the primary low-current GTAW cladding of Inconel 625 on 347 stainless steel alloy with varying the process parameters.

The general objective of this research is to understand the process parameter combination of hot-wire GTAW on forming the continuous and defect-free cladded bead. There are two specific objectives of this research. First, to understand the limitations of resistively heating wire in contrast to gas tungsten arc (GTA) and develop an analytical model for hot-wire current in order to pre-heat the wire. Second, to study the process parameters effect on the dilution as well

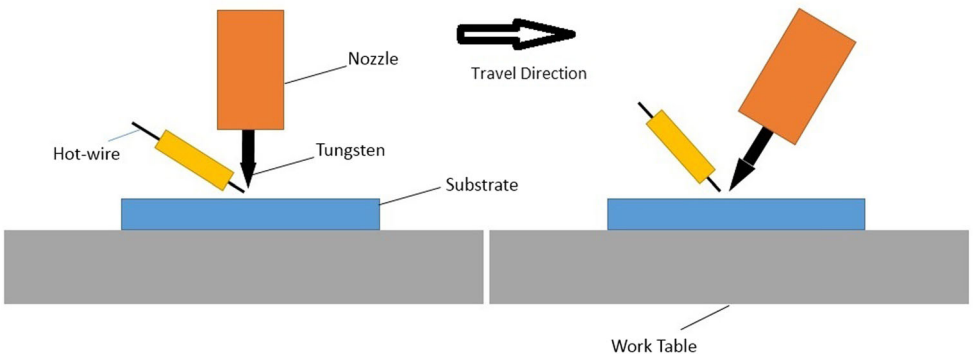

Fig. 2 Experimental setup of GTAW torch angle: standard feed angle (left) and vary angle (right)

Table 1 Chemical composition of the studied austentic stainless steel 347 (bal Fe) and Inconel 625 (bal Ni) filler wire [13, 14]

Alloy	Ni	Cr	Fe	Si	Mn	C	P	S	Nb	Mo
347 SS	11.0	18.0	Bal.	1.0	2.0	0.08	0.045	0.030	0.8	0.0
Inconel 625	Bal	20.0	5.0	0.5	0.5	0.1	0.015	0.015	3.15	8.0

as continuation of the bead surface by changing the orientation of cladding nozzle (Fig. 2). The orientation of nozzle has a significance in manual welding; however, it has not been studied in automated and mechanized welding. This paper brings significance to automated cladding and welding as well as the additive manufacturing industries. Some insights on microstructure evolution of both 347 stainless and IN625 have also been presented.

2 Experiment

2.1 Experimental setup

Multiple bead-on-plate experiments were performed with IN625 filler metal on a 12.7-mm 347 stainless steel. The length of the bead was 127 mm. The chemical composition of the substrate and the filler metal is shown in Table 1. The welding parameters are given in Table 2. The substrate was grind and cleaned with acetone prior to the experiment. A combination of experiments was performed varying primary current, hot-wire current, wire feed speed, travel speed (Table 2), and position of the GTAW torch (Fig. 2). A 6-axis robot was used in order to obtain the desired angle for the GTAW torch and maintain the constant travel speed. A 3-s pause was programmed in order to activate the tungsten and wire feed at start and end point of the long bead. The offset distance from the substrate to the tungsten tip and the distance from the filler wire to the tungsten was kept constant. A 100% Argon gas with flow rate of 15 lpm was used for shielding.

2.2 Sample characterization

The cladded specimens were sectioned with a wire EDM machine, grinded using SiC papers of 240–800 grit sizes, and thereafter polished with 1 micron alumina. The surface was etched with 15 mL hydrochloric acid, 10 mL acetic acid, and 5 mL of nitric acid. An optical microsturcture analysis was used to show the changes in interface between the clad and substrate. SEM and EDX analyses were performed to evaluate the Fe dilution.

3 Results and discussion

3.1 Effect of process parameter

3.1.1 Effect of torch angle

Figure 3 represents the effect of primary current and the torch angle on the continuity of the bead formation. At a primary current level of 80 A and higher, uniform and continuous beads were formed; the travel speed and wire-feed speed were 4 mm/s and 26.4 m/s, respectively, and the hot-wire current was 80 A. The selection of the travel speed and wire feed speed are determined to be within the limit of maximum deposition rate that can be achieved with such process. Within these parameters, the torch angle has no effect on the discontinuity of the bead formation as uniform and continuous bead was formed while varying the torch angle to the substrate. The current level of 70 A has discontinuous bead formation when the torch angle is perpendicular (90°) to the substrate. An inclination angle of 65 to 80° entails the continuity and uniformity in the bead formation. At lower current level (70 A and lower), wire dripping was observed, as the resistively heated wire does not spread out.

Even increasing the hot-wire current from 80 to 100 A did not suffice the continuous bead formation at a 70-A primary welding current. Although, the wire reaches close to the melting temperature due to higher hot-wire current, the melting of the substrate with the primary current was insufficient for the molten puddle to flow in the substrate. As expected, a further reduction in travel speed and substantial reduction in wire feed speed does allow the formation of continuous bead; however, a very thin clad layer was observed with lower wire feed speed.

Table 2 The welding parameters

Parameter	Primary current	HW current	Wire feed speed	Travel speed	Torch angle
Values	60–110 A	20–90 A	10–31 mm/s	2–5 mm/s	45 – 90°

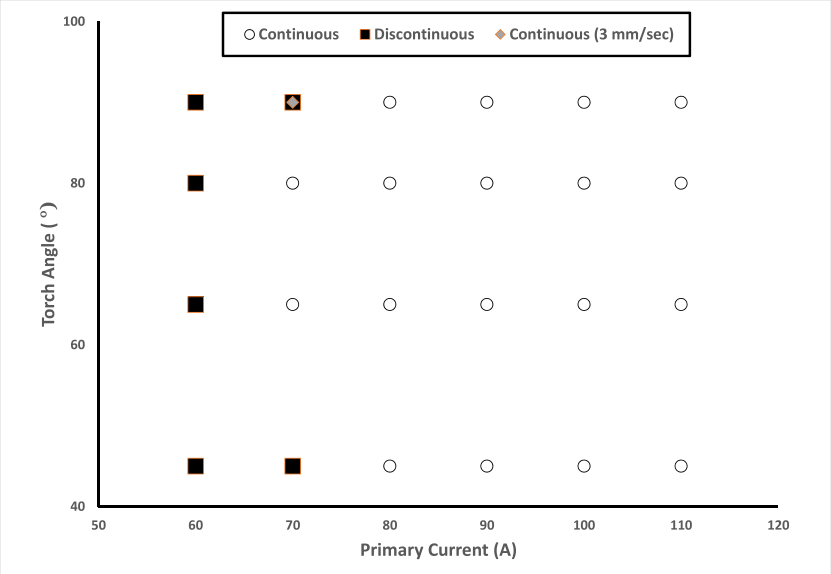

Fig. 3 The effect of primary current and the GTAW torch angle on the continuous and discontinuous bead formation

The cross-section specimens were extracted at the exact location within 40 mm from the starting point. The cross-section geometries and the bead-on-plate are shown in Fig. 4 for the 90° torch angle and primary current of 70, 80, 90, and 100 A respectively. The beads are continuous and uniform for 90° torch angle for primary current of 80 A, 90 A, and 100 A; however, wire dripping was observed in the middle as seen in the Fig. 4 for 70-A primary current. The continuity for some length for the 70 A is due to the high-frequency arc initiation system that imposes high voltage in the process. As the primary current drops, the geometric shape changes from wider to narrower; however, the non-uniform shape for primary current of 70 A was observed in Fig. 4 due to non-uniformity of the deposited clad layer.

Based upon the observation, it can be concluded that the inclination angle of GTAW has significant impact on

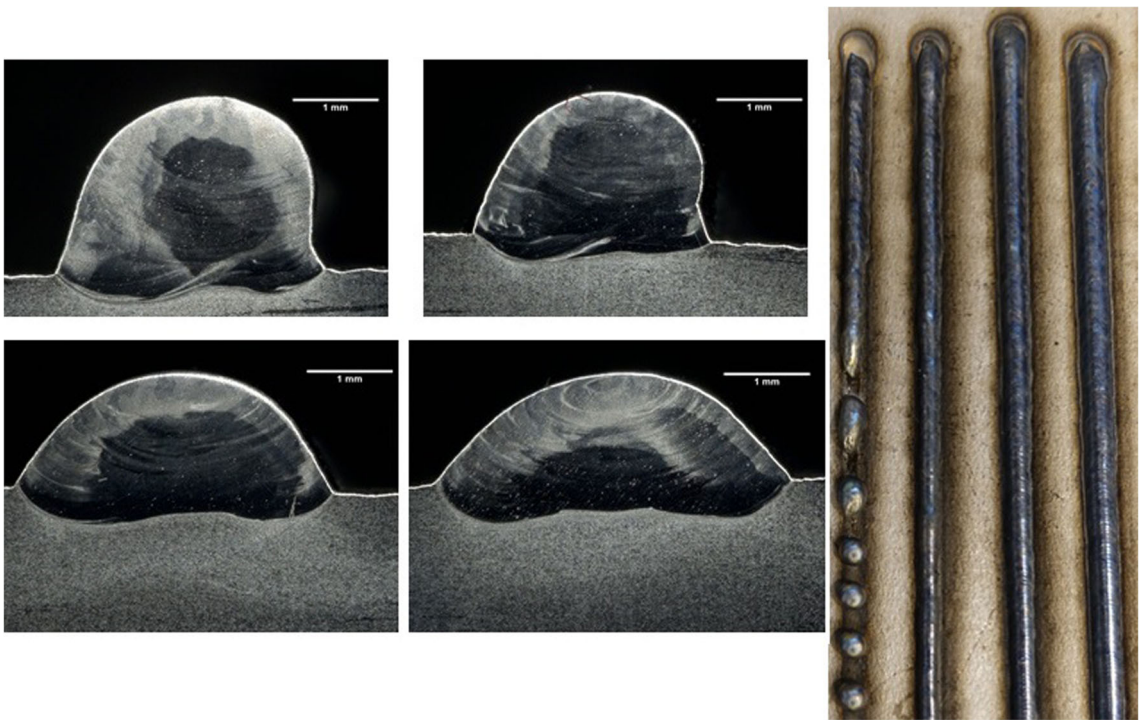

Fig. 4 The cross-section geometry of the cladded bead with respect to the primary current (left picture) 70 A (top left), 80 A (top right), 90 A (bottom left), and 100 A (bottom right); right picture 70 A (left), 80 A (middle), 90 A (middle), and 100 A (right); torch angle of 90°

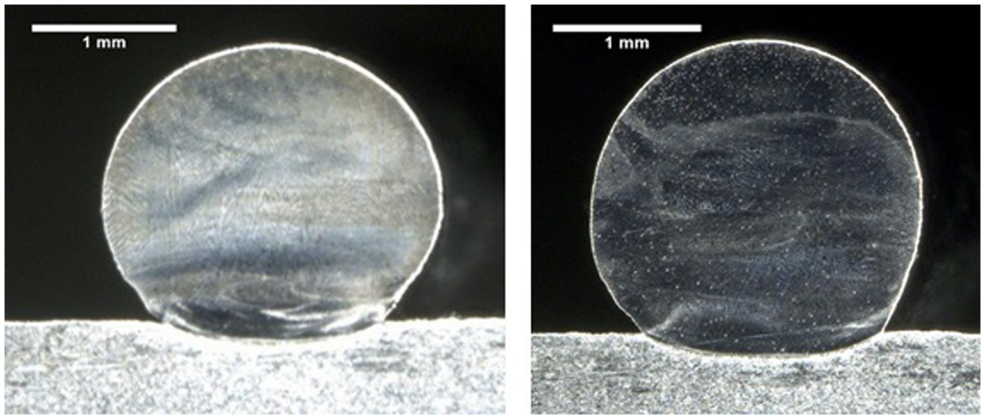

Fig. 5 The cross-section geometry of the cladded bead with respect to the torch angle (left picture 80° and right picture 65°); primary current of 70 A was used in both cases

the continuous bead formation allowing the molten metal to flow and spread out. In cladding and welding, an optimum interaction time is required to melt the substrate and spread/bond the filler metal. The higher interaction time is equivalent to the higher primary current and lower travel speed. A 70-A primary current is not enough to deposit a continuous layer with 90° torch angle. The torch angle in the range of 65 to 80° could be considered optimal angle to provide the continuous bead for the lower 70-A primary current. Figure 5 represents the cross-section geometry of IN625 by using 70-A primary current and 65 and 80° torch angle. A very low dilution has been observed which is further discussed in the section below.

There are two possible effects for the torch inclination angle in the low current cladding. First, the heat energy will not concentrate vertically downward, this will reduce the penetration and thus dilution in the weld. Moreover, it enlarges the heating zone as more heat will be radiate ahead of the welding direction and pre-heats the substrate. This has also been validated by the work performed by [15], as their results suggest a wider heating zone while tilting the torch. Second, due to the effect of the shielding gas pressure on the molten puddle, the angle of $65 - 80°$ exerts component velocities on both the horizontal and vertical directions which helps to spread out. Both the melt depth and width are important for the filler wire to be in contact and spread out to form continuous and uniform bead.

3.1.2 Effect of hot-wire current

The melting of filler wire in cold-wire GTAW with less than 100-A primary current is not possible as the radiating heat is not sufficient to melt the wire. A reasonable (lower) travel speed (1–4) mm/s and wire feed speed within the primary current range (70–75 A) is not sufficient as the un-melted wire will stick into the puddle. At relatively low wire feed speed of 11 mm/s, the short-circuit transfer occurs and a thin layer of clad will form on the substrate at a primary current of 70 A. Increasing the wire feed speed greater than 25 mm/s does not produce the uniform clad within 0 to 5 degree torch angle. A hot-wire current less than 50 A is not sufficient to melt the wire, as the wire will stick into the puddle similar to cold-wire GTAW. A higher hot-wire current does reach the melting temperature of the wire; however, within the small range of primary current (70–80 A), it is not possible to clad a continuous bead. At very high hot-wire current, a phenomenon known as magnetic arc blow occurs. A magnetic arc blow is the phenomenon that occurs due to electromagnetic interaction between hot-wire current and primary arc current, which complicates the welding process as explained by Hori et al. [16]. Thus, the suitable range of hot-wire current for low-current cladding will be 70 to 80 A. Although the wire will reach closer to the melting temperature prior to clad, the fluidity of the molten wire is dependent upon the overall melt surface depth and width on the substrate, as well as the cooling rate, thickness of the substrate, and thermal diffusivity of the material. This is a primary reason for resistively heating the wire and melting process is not sufficient to deposit a continuous layer.

It is very important to understand the effect of resistively heating wire on the wire temperature before it enter the melt pool. An analytical model using energy balance method [17] neglecting the convection and radiation losses is compared with experimental results. The experiment was performed by using a Micro-Epsilon infra-red thermometer to record the temperature at 5 Hz when the wire strikes the substrate without using the GTAW arc. Both the length and the wire-feed speed are made constant, thus the heating time is independent of the length and wire feed speed. In case of resistively heating the wire, the process involves passing a direct electrical current with resistance R (depends upon the wire geometrical and resistivity). Using conservation of energy,

$$m * C * \frac{dT}{dt} = I^2 * R \tag{1}$$

where m is the mass, C is the specific heat, dT is the temperature difference and equals to $T_2 - T_1$, dt is the

Table 3 The room temperature material properties of IN625 used for hot-wire temperature formulation

Parameter	Radius of wire	Density	Resistivity	Specific heat	Length
Values	0.0445 cm	8.44 gm/cm^3	$0.129 * 10^{-6} \Omega m$	410 $\frac{J}{KgK}$	31.75 mm

time difference to reach the temperature of T_2 from room temperature T_1, and I is the hot-wire current.

Integrating and rearranging the equation,

$$\int_{T_1}^{T_2} dT = \frac{I^2 * R}{m * C} \int_0^t dt \tag{2}$$

The resistance, density, and the specific heat are the functions of temperature, thus these values will have some impact on temperature changes; however, in this calculation, constant room-temperature physical properties are used. The properties used are presented in Table 3. It is well-known from this equation that the temperature of the wire is directly proportional to the square of the hot-wire current. Figure 6 represents the theoretical and experimental results of the pre-heat temperature. As seen, increasing the hot-wire current will increase the temperature; however within the limit of the hot-wire feeder, up to 100 A, the wire will not quite reach the melting temperature of the alloy. In addition, the temperature is dependent upon the rate at which the wire will reach the higher temperature from the room temperature. The response time to reach the maximum temperature is dependent upon the wire feed speed and extension as described by [17]. At higher current, due to surface tension and the filler wire striking on the substrate, the wire breaks, thus it never reaches the steady state value of the set current. This is the main reason, there is no significant difference in temperature when the hot-wire current is 58 A and 90 A as depicted in Fig. 6.

3.2 Dilution

The contact angle (wetting angle), which is proportional to the clad height and the width, has been determined and depicted in Fig. 7. The contact angles are all less than 80°, suitable for cladding application according to [5]. The DR decreases with respect to the primary current. A decreasing width, aspect ratio (width/height), and increasing contact angle were observed when the primary current was decreased. The deviation in the aspect ratio and contact angle for the primary current of 70 A was mainly due to the uneven clad surface deposited due to lower primary current.

The dilution ratio (DR) is the percentage of the total area of the substrate material in the weld contributed by melting of substrate. The following equation has been used to calculate the dilution ratio.

$$DR = \frac{A_F}{A_F + A_S} \tag{3}$$

where A_F is the area of the substrate melted and A_S is the area of filler metal added. In contrast to welding where higher DR is desired, it is widely believed that a lower DR is desired in cladding to avoid the elemental segregation. It is obvious from Fig. 7 that the DR is higher for the primary current of 100 A. The DR are 20–30% for 90 and 100 A while 10–15% for 70 and 80 A; however, a significant drop in dilution was observed when the torch angle was reduced to $65 - 80°$ (Figs. 7 and 5). The EDX analysis discussed in the next section also reveals the higher Fe dilution for higher level of current.

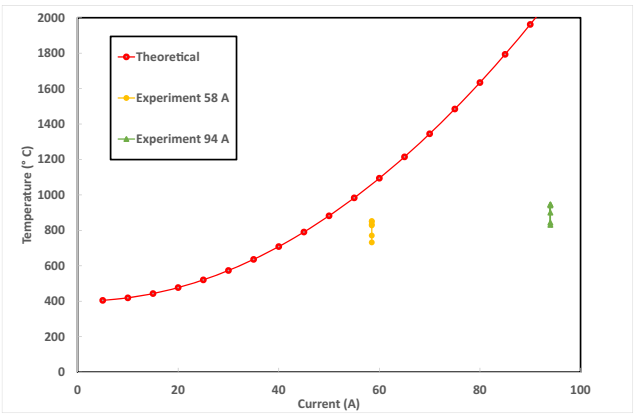

Fig. 6 Theoretical and experimental results of the resistively heating temperature of IN625 alloy

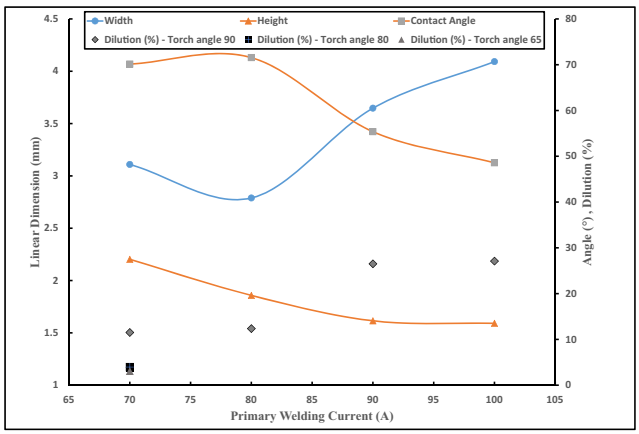

Fig. 7 The clad bead width, height, contact angle, and dilution with respect to primary current

3.3 Microstructure analysis

3.3.1 Microstructure of IN625

Figure 8 represents the as-cladded microstructure in a cross section perpendicular to the hot-wire GTAW cladding direction for 70- and 90-A primary current. The microstructure mostly consist of columnar dendrites which has epitaxial growth from the substrate typical to the welding [18] for all cases. It is worth noting that the grain direction is not exactly perpendicular to the welding direction. The middle region shows coarse dendritic structure with secondary dendrite arms as depicted in Fig. 8. Some dendrite fragments are also present in the microstructure (Fig. 8). Similar results were obtained by [19] and [20] while cladding IN625. This is mainly due to the local solidification rate and temperature gradient during the cladding process as the ratio of temperature gradient to solidification rate will determine the grain morphology after the solidification [21]. The average primary dendrite spacing is 15 micron, while the secondary dendrite spacing is between 4–8 micron. These values are similar or less than the values presented by [20] while using laser and wire.

3.3.2 Microstructure of 347 stainless steel

347 stainless steel is the stabilized grade containing small additions of niobium to combine with carbon and reduce the tendency for intergranular corrosion. The interface between IN625 and 347 stainless steel and the microstructure of the 347 stainless steel are presented in Fig. 9. The darker region in the image represents the deformed surface slightly below the fusion line. The microstructure consists of austenitic matrix with equiaxed grains. Annealing twins can be observed in the austentic matrix. There is no significant difference in the grain size of the HAZ; however, it seems the darker region has decreased when the the primary current has increased from 70 to 100 A, which entails the lack of fusion when the primary current is at lower extreme.

The scanning electron microscopy of the interface reveals the crack in the coarse grained heat–affected zone (CGHAZ) of 347 stainless steel for primary current level of 90 A and 100 A. No crack was observed for the primary current level of 70 and 80 A. The crack in the heat-affected zone (HAZ) seems to be intergranular, formed when in contact with the etchant (Fig. 10). This type of crack occurs due to constitutional liquation [22] . The rapid heating induces the formation of localized liquation in eutectic Nb(C, N). This might be the primary reason for the crack to appear in the specimen. It is also evident that temperature near 723 to 1123 K, there is higher chance of forming chromium carbide than niobium carbide [23] due to dissolution of Nb(C, N). The liquation crack initiates in a grain boundary of the CGHAZ and propagates when reacted with chlorine ion from the etchant. An EDX analysis reveals the formation of in homogeneous niobium carbonitride Nb(C, N) at many locations (Fig. 11), which entails the microsegregation of niobium-rich liquation bands and liquation cracks occurs at the grain boundaries supported by the work performed by [24]. Based upon the results, it can be concluded that the temperature range experienced under 70 to 80 A is less susceptible for the HAZ cracking in 347 stainless steel due to the low cooling rate.

3.3.3 EDX analysis

The chemical composition of base metal is different from the deposited wire 2. The unmixed zone of dissimilar metal joint was at the boundary between two alloys. A chemical composition mapping can also be used to calculate

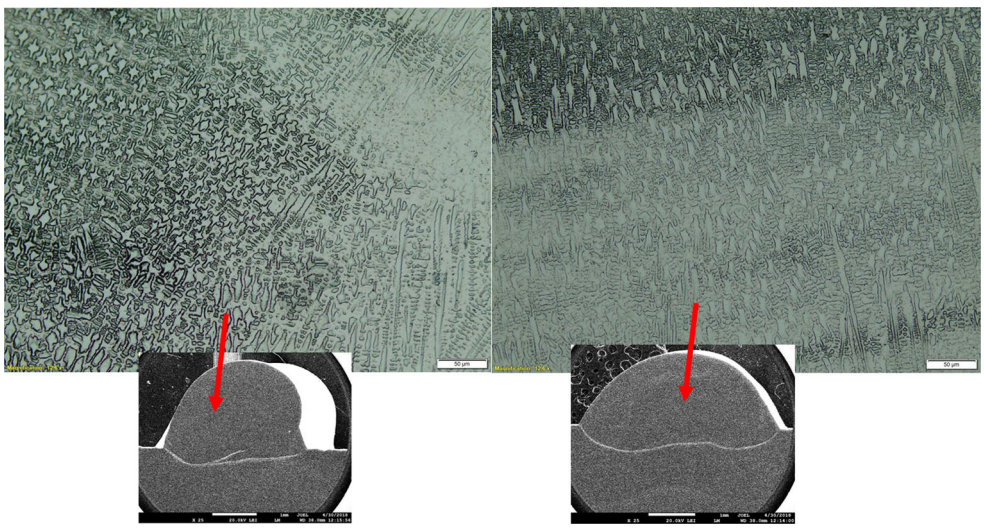

Fig. 8 Microstructure of middle-corner region of IN 625 deposited by 70-A primary current (left) and 90-A primary current (right)

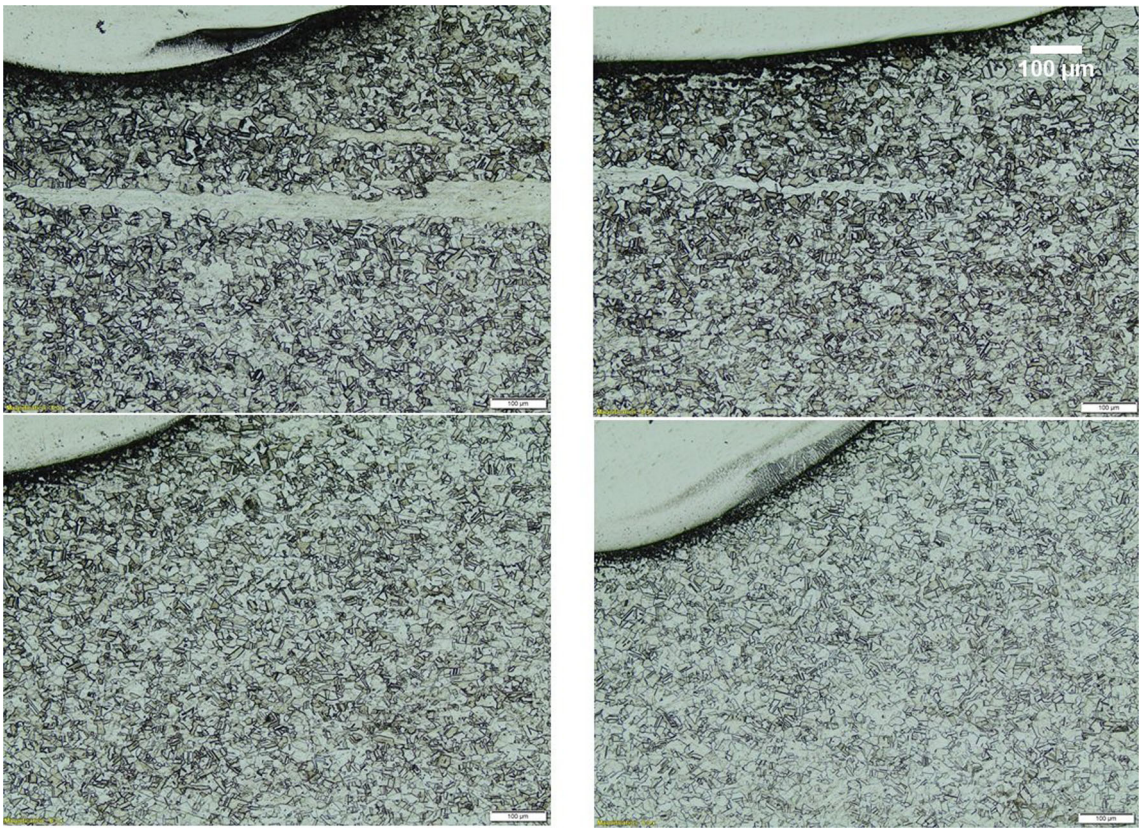

Fig. 9 The representative microstructure of 347 stainless steel 70 A (top left), 80 A (top right), 90 A (bottom left), and 100 A (bottom right)

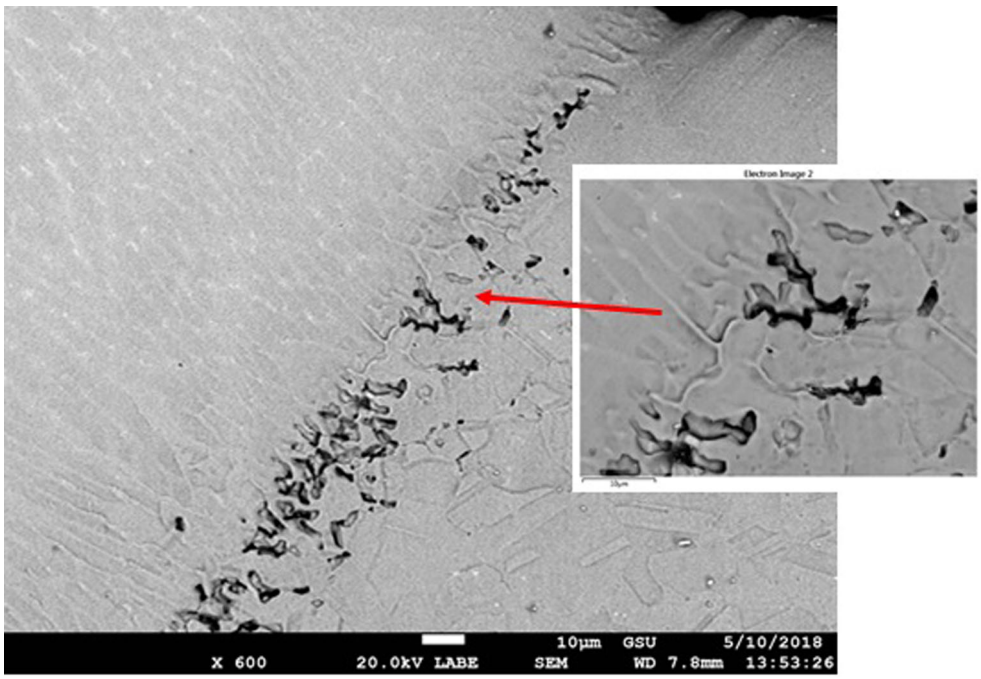

Fig. 10 HAZ cracking observed on the 100-A cladded 347 stainless steel (left), higher magnification (right)

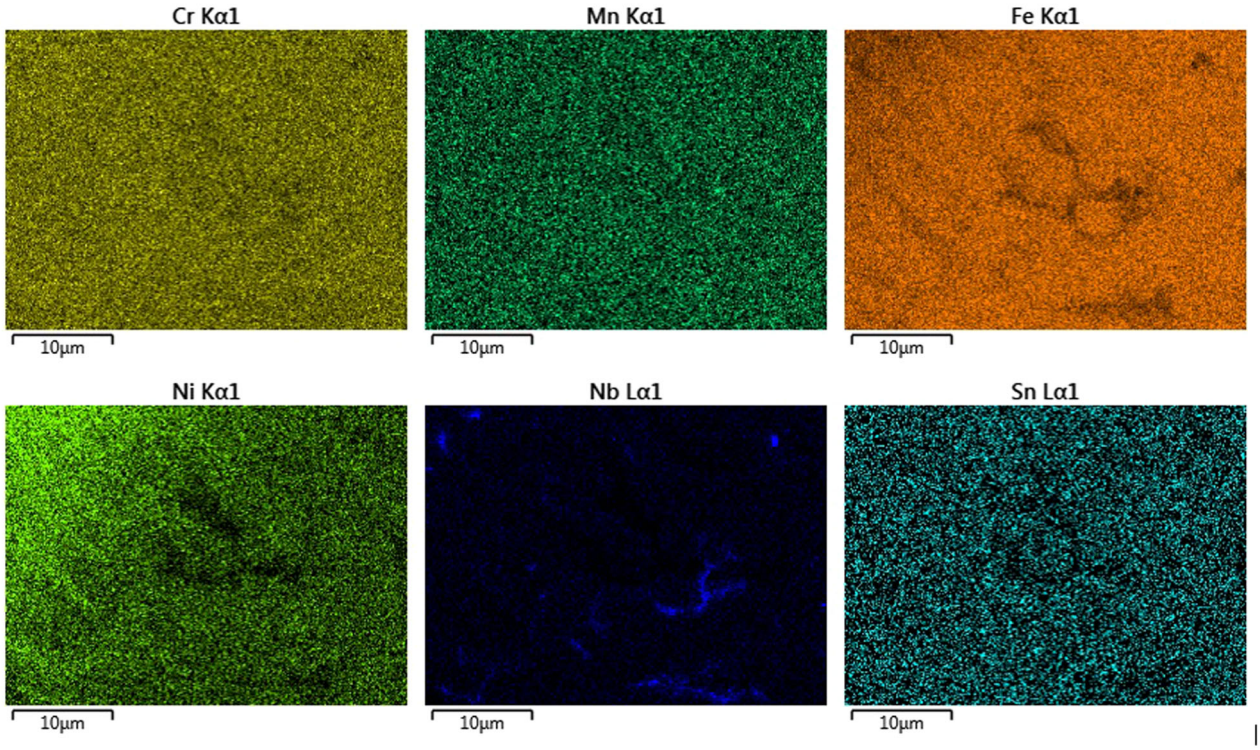

Fig. 11 Representative EDX elemental mapping of the crack region in Fig. 10

elemental dilution [25]. An EDX analysis (Fig. 12) was performed in order to evaluate the Fe dilution on the clad material. The chemical composition analyzed by EDS reveals the gradual increment of alloying element. As seen in the diluted (melted) region in Fig. 12, the Fe content is 30.2% for 90-A primary GTAW current. The IN625 has only 5% Fe content. The lower primary current 70 and 80-A reveals a lower Fe content of 17–20% in the diluted region. This is significantly less than using shielding metal arc welding [9] and nearly equal to laser cladding [20]. The higher Fe content is responsible to lower resistance to corrosion as depicted by [5]. The EDX analysis reveals the

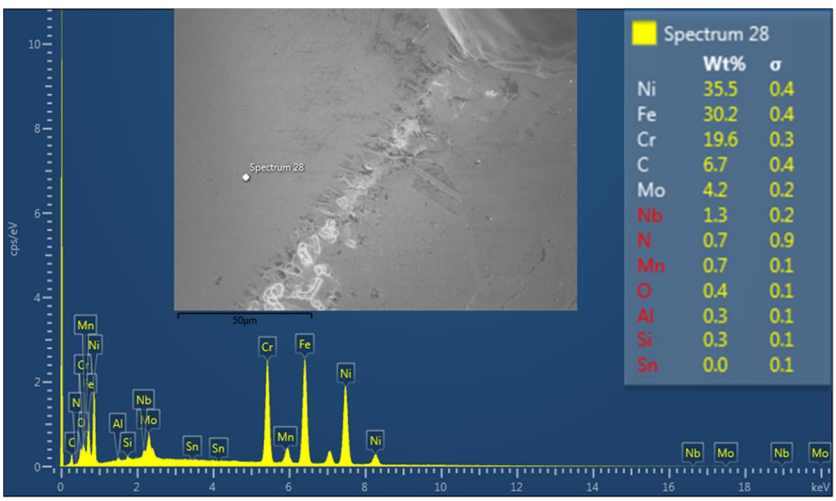

Fig. 12 The observation of Fe dilution on the melt region by EDX analysis performed on the sample by using 90-A primary GTAW current

increasing trend in dilution of Fe when the primary current is increased, equivalent to the dilution ratio (DR). The melt pool depth is also higher for 100-A clad (Fig. 4). Thus, it can be concluded that the higher primary current, the higher the Fe content onto the clad surface.

4 Conclusion

A theoretical hot-wire filler temperature relationship has been used to validate the experimental temperature measurements.

A 70 A is the minimum primary current required to have a continuous bead formation. The effect of torch angle has significance on the continuity of the bead formation at low primary current level.

The lower heat input results in minimum dilution as well as minimum Fe dilution on the cladding. It seems that the studied current range 90–100 A has an effect on the formation of liquation cracking on the heat-affected zone (HAZ) of 347 stainless steel.

Acknowledgements The authors would like to thank Mr. Frank Qualls for helping and obtaining SEM and EDX results. The authors would also like to thank Mr. Michael Santangelo for providing the welding supplies and for a thoughtful discussion.

Funding information This work has been financially supported by Georgia Southern Office of Research Services and Sponsored Programs (ORSSP).

References

1. Xu G, Kutsuna M, Liu Z, Yamada K (2006) Comparison between diode laser and tig cladding of co-based alloys on the sus403 stainless steel. Surf Coat Technol 201(3-4):1138–1144
2. Silwal B, Santangelo M (2018) Effect of vibration and hot-wire gas tungsten arc (gta) on the geometric shape. J Mater Process Technol 251:138–145
3. Källqvist J, Andrén HO (1999) Microanalysis of a stabilised austenitic stainless steel after long term ageing. Mater Sci Eng A 270(1):27–32
4. Lippold J, Baeslack W, Varol I (1988) Heat-affected zone liquation cracking in austenitic and duplex stainless steels. Weld J (USA) 71(1):1
5. Abioye T, McCartney D, Clare A (2015) Laser cladding of inconel 625 wire for corrosion protection. J Mater Process Technol 217:232–240
6. Adamiec J (2009) High temperature corrosion of power boiler components cladded with nickel alloys. Mater Charact 60(10):1093–1099
7. Dinda G, Dasgupta A, Mazumder J (2009) Laser aided direct metal deposition of inconel 625 superalloy: microstructural evolution and thermal stability. Mater Sci Eng A 509(1-2):98–104
8. Abioye T, Folkes J, Clare A (2013) A parametric study of inconel 625 wire laser deposition. J Mater Process Technol 213(12):2145–2151
9. Sandhu SS, Shahi A (2016) Metallurgical, wear and fatigue performance of inconel 625 weld claddings. J Mater Process Technol 233:1–8
10. Pajukoski H, Näkki J, Thieme S, Tuominen J, Nowotny S, Vuoristo P (2016) High performance corrosion resistant coatings by novel coaxial cold-and hot-wire laser cladding methods. J Laser Appl 28(1):012011
11. Lv S, Xu Z, Wang H, Yang S (2008) Investigation on tig cladding of copper alloy on steel plate. Sci Technol Weld Join 13(1):10–16
12. Günther K, Bergmann JP, Suchodoll D (2018) Hot wire-assisted gas metal arc welding of hypereutectic fecrc hardfacing alloys: microstructure and wear properties. Surf Coat Technol 334:420–428
13. RolledAlloys (2011) Data sheet. https://www.rolledalloys.com/shared-content/technical-resources/datasheets/347_DS_US_EN.pdf, Accessed: 2018-11-30
14. RolledAlloys (2011) Data sheet. https://www.rolledalloys.com/shared-content/technical-resources/datasheets/625_DS_US_EN.pdf, Accessed: 2018-11-30
15. Parvez S, Abid M, Nash D, Fawad H, Galloway A (2012) Effect of torch angle on arc properties and weld pool shape in stationary gtaw. J Eng Mech 139(9):1268–1277
16. Hori K, Watanabe H, Myoga T, Kusano K (2004) Development of hot wire tig welding methods using pulsed current to heat filler wire–research on pulse heated hot wire tig welding processes. Weld Int 18(6):456–468
17. Wei H, Zhang Y, Tan L, Zhong Z (2015) Energy efficiency evaluation of hot-wire laser welding based on process characteristic and power consumption. J Clean Prod 87:255–262
18. David S, Babu S, Vitek J (2003) Welding: solidification and microstructure. Jom 55(6):14–20
19. Xu X, Mi G, Chen L, Xiong L, Jiang P, Shao X, Wang C (2017) Research on microstructures and properties of inconel 625 coatings obtained by laser cladding with wire. J Alloys Compd 715:362–373
20. Feng K, Chen Y, Deng P, Li Y, Zhao H, Lu F, Li R, Huang J, Li Z (2017) Improved high-temperature hardness and wear resistance of inconel 625 coatings fabricated by laser cladding. J Mater Process Technol 243:82–91
21. Kou S (2003) Welding metallurgy, New Jersey, USA pp 431–446
22. Li L, Messler RW (2002) Dissolution kinetics of nbc particles in the heat-affected zone of type 347 austenitic stainless steel. Metall and Mater Trans A 33(7):2031–2042
23. Fukunaga T, Kaneko K, Kawano R, Ueda K, Yamada K, Nakada N, Kikuchi M, Barnard JS, Midgley PA (2014) Formation of intergranular m23c6 in sensitized type-347 stainless steel. ISIJ Int 54(1):148–152
24. Bai G, Li Y, Lu S (2018) Localized liquation and resultant pitting corrosion behavior of welding coarse-grained heat-affected zone in niobium-stabilized austenitic stainless steel. J Electrochem Soc 165(11):C722–C731
25. Abioye T, Farayibi P, McCartney D, Clare A (2016) Effect of carbide dissolution on the corrosion performance of tungsten carbide reinforced inconel 625 wire laser coating. J Mater Process Technol 231:89–99